Optica Applicata, Vol. LIV, No. 4, 2024
DOI: 10.37190/oa/195222

Dual resonance self-referenced refractive index sensor using 2D silicon photonic crystal cavity waveguide system

NILAKSHA GHOSH, PUJA SHARMA, SARANG MEDHEKAR*

Department of Physics, Central University of Jharkhand, Ranchi, India

*Corresponding author: sarang.medhekar@cuj.ac.in

In this work, we have designed and simulated a dual resonance self-referenced refractive index sensor using two dimensional “silicon rods in air” photonic crystal. The proposed sensor uses two wavelengths, namely sensing wavelength and the reference wavelength, to measure the change in the transmission of light with respect to the change in refractive index. It is shown that a change of refractive-index of the photonic crystal rods (in the range of 3.46–3.466) causes a significant change in transmission of the sensing wavelength, while, transmission of the reference wavelength remains almost same. This method of sensing is more efficient in gauging the impact of external factors on the results generated by the sensor. The proposed sensor exhibits a fairly high sensitivity and quality factor of 9912.85%/RIU and 708.17, respectively. The device is compact in size making it portable and hence suitable for field applications. Most of the self-referenced refractive index sensors use wavelength shift to measure different parameters but in the present paper we have used the difference of transmission between two (sensing and reference) wavelengths at a particular refractive-index to calculate the performance of the sensor.

Keywords: photonic crystal, FDTD, PWE, self-referenced, refractive-index sensing.

1. Introduction

The present decade has seen a rapid progress of optical technologies in the fields of communication and sensing. Silicon based optical devices in particular have undergone a lot of development in the past couple of decades [1-7]. Silicon photonic crystals (PhCs) have emerged as very promising candidates for these optical devices mainly due to their potential to realize highly compact devices with high accuracy. PhCs are uniform dielectric nano structures and plenty of proposals on PhC based devices can be found in literature [8-17]. Refractive index (RI) based optical sensors have become one of the most useful devices in the past few years for the purpose of structural monitoring and label free detection [18-24]. Factors like enhanced sensitivity, compact size, robustness and immunity from electromagnetic interference make RI based optical sensors a very lucrative field of research and hence, a lot of recent research efforts are focused on self-referenced RI sensing [25-38]. ZHANG *et al*. experimented with the idea of a self -referenced biosensor as early as 2013 [31]. SRIVASTAV *et al*. investigated the possibility of a surface plasmon resonance based self-referenced sensor using indium tin oxide film in great detail and WANG *et al*. in 2017 experimented with the idea of a double Fano resonance based self-referenced plasmonic sensor [28,35]. VERMA, SRIVASTAV and PAN, SRIVASTAV presented a work on plasmonic self-referenced refractive-index sensor in the near infrared communication band [34,37]. SUN *et al*. examined the idea of self-referenced sensing in all-dielectric structure in 2020 [38]. More recently CHOWDHURY *et al*. have explored self-referenced sensing utilizing Tamm plasmon polariton in photonic quasicrystals [26]. In case of self-referenced RI sensing, two wavelengths are used out of which one undergoes adequate changes, in terms of its transmission or resonant wavelength with the variation in RI (referred as the reference wavelength), while, the other frequency shows negligible change (referred as the reference wavelength). This method of sensing helps to gauge and compensate for external factors (humidity *etc*.) without the requirement of any external reference [36].

In the present work, we have designed and simulated intensity based dual resonance self-referenced RI sensor using 2D silicon (Si) rods in air type PhC. While most of the self-referenced sensors uses shift of resonant wavelength to measure the different parameters, in the present work we have used the variation of transmission to gauge the performance of the proposed device. Most of the self-referenced refractive index sensors are for chemical and biological analyte sensing and they use plasmonic and quasi photonic crystals, while, the proposed sensor in the present paper is a pressure and temperature sensor designed on a dielectric PhC.

The proposed sensor shows a sensitivity of 9912.85%/RIU and a quality factor of 708.17. The sensitivity of the designed sensor is calculated using the transmission difference between two wavelengths, *i.e.* the sensing wavelength and the reference wavelength for a change in the RI of the silicon rods, instead of measuring the resonant wavelength shift. It is worth to mention here that most of the self-referencing structures existing in the literature are layered structures, however, the structure proposed in the present paper is a waveguide-cavity system.

2. Basic PhC structure

PhCs are nanometer dimension periodic structures with the period being smaller than the wavelength of light. PhCs offer photonic band gap (PBG), the range of frequencies which propagation is prohibited through them [39]. The concept of PBG can be understood as a destructive interference effect of multiple reflection of light at the interface of two contrasting RI region, i.e region of high and low RI. The Maxwell's equation to describe light propagation through PhCs is given by [40]

$$\nabla \cdot [\nabla \cdot E(r)] = \left(\frac{\omega}{c}\right)^2 \varepsilon(r)$$

Here, $\varepsilon(r)$ denotes the dielectric function, r is the position vector, c is the velocity of light and ω is the angular frequency.

The PBG of a structure is dependent on parameters like the lattice constant, lattice structure, radius of the holes or rods and the RI of the material. Location and width of PBG of a given structure is determined by inserting above mentioned parameters in the Maxwell's equation which also determines whether the structure allows for the propagation of TE or TM waves. By introducing defects in the PhC structure, forbidden frequencies can be guided to transmit through the structure.

The Maxwell's equation can be solved using the frequency domain or time domain methods like the finite difference time domain (FDTD) [40] or the plane wave expansion (PWE) [41] methods. While, FDTD is used for simulation of light propagation through the considered structure, the PWE is used to calculate the PBG of the structure. The basic platform/structure in the present work is the periodic arrays of silicon rods in square lattice with air as the background material as shown in Fig. 1. The high contrast

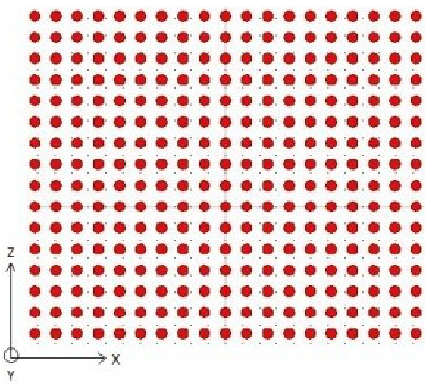

Fig. 1. Basic photonic crystal structure considered here.

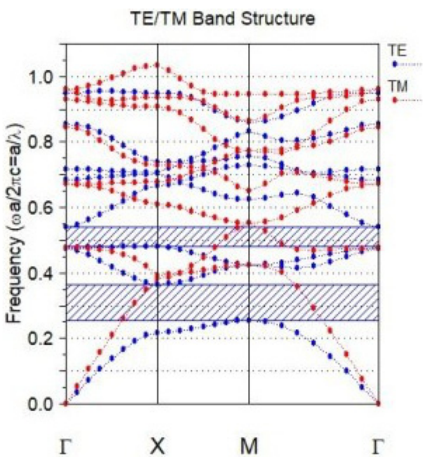

Fig. 2. Band diagram of the considered photonic crystal structure.

between the silicon (RI = 3.46) and air (RI = 1) allows for strong confinement of light in the structure making the device very compact. In case of 2D (two dimensional) PhC, the RI contrast takes place along the *xz*-plane and remains unchanged along the *y*-axis, so the light is confined in the *xz*-direction. The other parameters are chosen as the lattice constant $a = 0.62$ μm and the radius of the rods $r = 0.15$ μm. The chosen parameters result in the band diagram of the basic structure (obtained using RSoft-CAD software) as shown in Fig. 2. It can be observed in the figure that the structure offers two band-gaps for TE modes. The first bandgap lies in the range $0.259 \leq a/\lambda \leq 0.36$ while the second in the range $0.48069 \leq a/\lambda \leq 0.5433$. The wavelength of our interest lies in the first band. What follows is the details of the sensor structure created on the above-mentioned basic platform.

3. Sensor structure

The sensor structure consists of two defect waveguides WG1 and WG2 coupled through a PhC cavity (encircled) as shown in Fig. 3. These defect waveguides are formed by removing the Si rods as shown. The cavity is formed by changing the radius of five PhC rods labelled as r_a, r_b, r_c and r_d as shown. Here $r_a = 0.35$ μm) are the scattering rods. The structure has one input port at WG1 and one output port at WG2 as shown. The chosen radii of the other rods of the cavity are $r_b = 0.09$ μm, $r_c = 0.07$ μm and $r_d = 0.05$ μm.

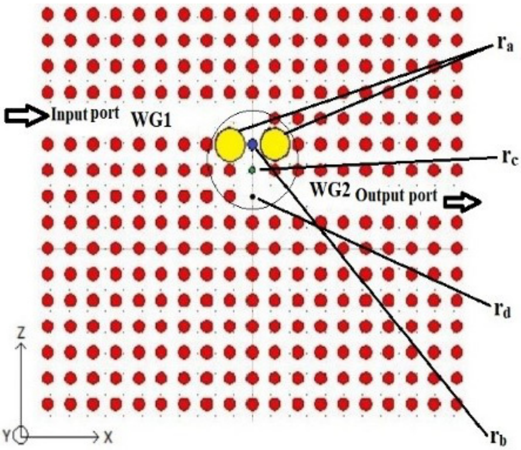

Fig. 3. Structure of the proposed sensor.

4. Numerical investigations and results

Numerical investigations are performed using the 2D-FDTD method. A perfectly matched layer (PML) of 500 nm is assumed to avoid the problem of back reflections from the boundary of the simulation domain. RSoft-CAD software is used to carry-out the required simulations. From the band diagram (Fig. 2) it is clear that the structure allows for the propagation of TE modes. Further, no propagation takes place in the y-direction ($\partial/\partial y = 0$), therefore only three components *i.e.*, E_y, H_x, H_z are considered for the 2D-FDTD simulations.

In the first step of our investigations, a wide spectrum Gaussian pulse is considered to be lunched in to the input port and its spectral response is noted at the output port. The sensing wavelength λ_s and the reference wavelength λ_r are chosen which are corresponding to the two peaks of the of the spectral response.

In the second step, the chosen wavelengths are considered to be injected into the structure and the change in their transmission with variation of RI is monitored. The RI of the silicon rods are varied from 3.46 to 3.466 in the steps of 0.001.

The formula used to measure the transmission function is [11]

$$T(f) = \frac{0.5\,\mathrm{real}(p(f)^{\mathrm{monitor}})ds}{\text{input power}}$$

where $T(f)$ is a function of wavelength, $p(f)$ is the Poynting vector and ds is the surface normal. A grid size of $a/20 = 31$ nm and time step of $\Delta t = 0.0195$ has been used to perform the FDTD simulations. The time-step is calculated using the following formula [18]

$$\Delta t \leq \left[c\sqrt{\frac{1}{(\Delta x)^2} + \frac{1}{(\Delta y)^2}} \right]^{-1}$$

The sensitivity of the proposed RI sensor is calculated using the formula $S = \Delta T/\Delta n$, here ΔT is the transmission difference, $\Delta T = |T_s - T_r|$ where I_R and I_S are the intensities of the λ_R and the λ_S at a particular RI. The quality factor Q of the sensor is calculated using the formula $Q = \lambda_s/\mathrm{FWHM}$ [18], FWHW represents the full width at half maximum.

The spectral response obtained, in the range 1.76 to 1.845 μm, with considered parameters is as shown in Fig. 4.

There are two peaks in the spectral response, one is very sharp, while the other is very broad. We chose wavelength corresponding to the sharp peak as our sensing wavelength λ_s, while the same corresponding to the broad peak is the reference wavelength λ_r. It can easily be anticipated from Fig. 4 that the sharpness of the sharp peak decides about the sensitivity of the sensor, while, broadness of the broad peak decides that the extent the self-referencing remains unperturbed with the external factors. Therefore, sharp peak of very high-quality factor is always desirable. The above mentioned will be clearer in the following part of the discussion. It is worth to mention that sensors with higher and higher sensitivity need optical sources of more and more stable output (lesser and lesser output fluctuations).

The parameters chosen here result in the sharp peak of the spectral response with highest quality factor. To show it, we present the effect of change of (i) lattice constant (ii) radius of scattering rods, and (iii) RI of all the rods on the spectral response.

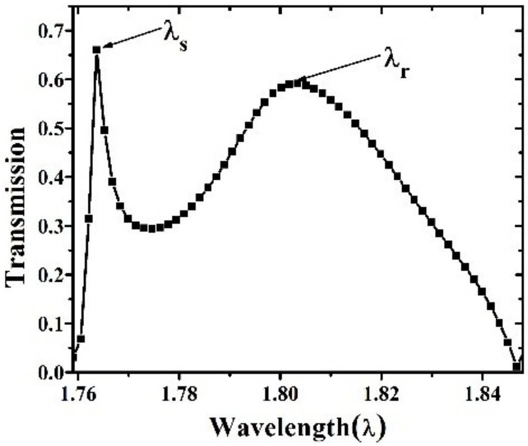

Fig. 4. Spectral response of the proposed sensor in the range of 1.76 to 1.845 μm.

The spectral response obtained for different lattice constants is shown in Fig. 5 and corresponding quality factors in Fig. 6. It is observed in Fig. 5 that the curve of the spectral response shows a redshift as the lattice constants is varied from 0.6 to 0.63 μm. We found that the quality factor of 708.17 of the sharp peak is obtained for the lattice constant of 0.62 μm which is highest among the same obtained for other lattice constants. Figure 7 shows spectral response for different radii of the scattering rods. It is evident in the figure that sharp peak of the spectral response is sharpest when the radius of the scattering rods is 0.35 μm. Hence, our chosen parameters (see Fig. 3) are justified as the most suited parameters giving us best possible spectral response (as in Fig. 4).

To investigate refractive index sensing, we investigated the effect of change in RI of the all the rods on the spectral response. The result is as shown in Fig. 8. Figure 8 shows shift in the spectral response of Fig. 4 with change in RI.

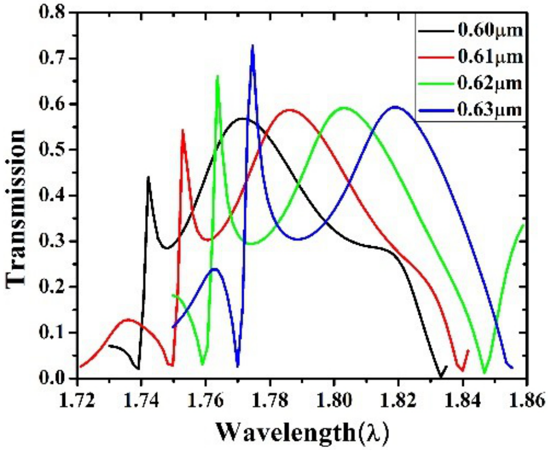

Fig. 5. Spectral response for different lattice constants.

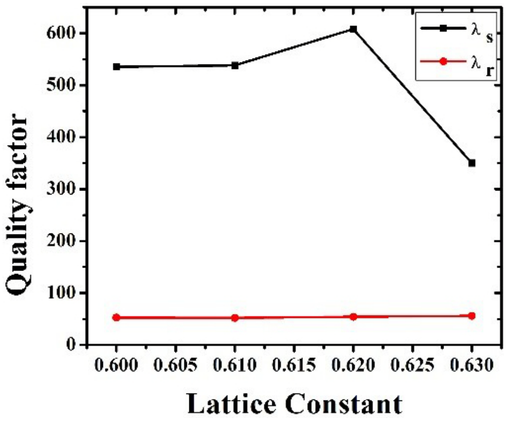

Fig. 6. Quality factor of sharp and broad peaks for different lattice constants.

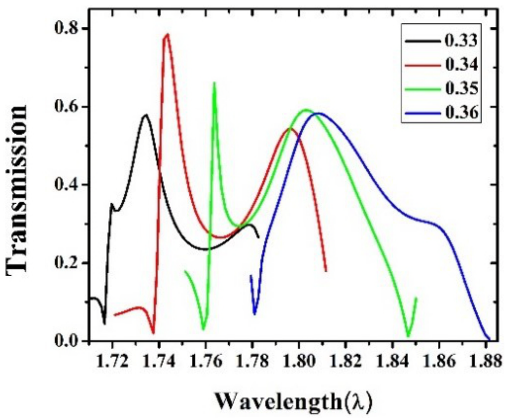

Fig. 7. Spectral response for different radius of scattering rod.

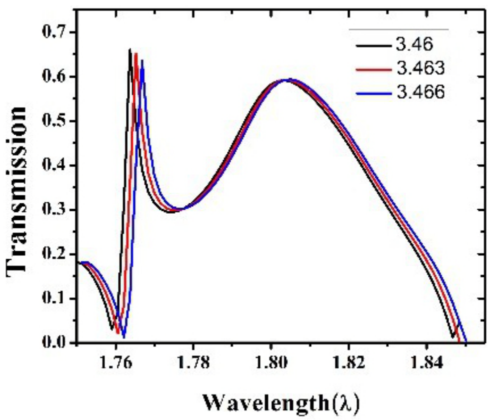

Fig. 8. Spectral response for different refractive-index of the rods.

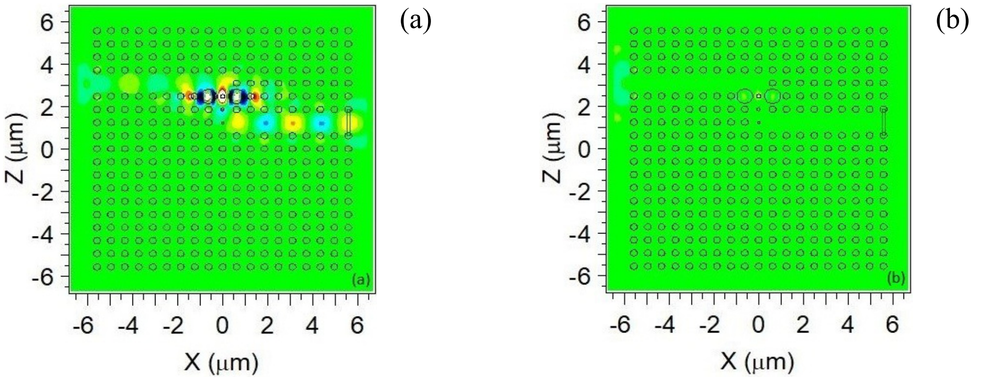

Fig. 9. Light propagation in the structure for 1.7637 μm (λ_s) when (a) RI = 3.46, and (b) RI = 3.466.

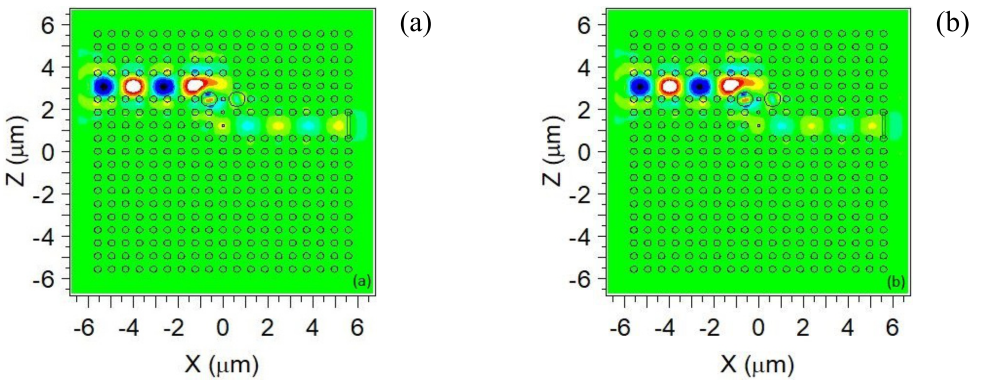

Fig. 10. Light propagation in the structure for 1.8033 μm (λ_r) when (a) RI = 3.46, and (b) RI = 3.466.

The functioning of the sensor can easily be understood from the Fig. 4 and Fig. 8. The sharp peak of Fig. 4 has a quality factor of 708.17, while, the broad peak of 54.15. Clearly a small shift in the spectral response (due to change in the RI of 0.003) should cause a significant change in transmission of λ_s, while there would be hardly any change in transmission of λ_r. To confirm our anticipation, we injected λ_s = 1.7637 μm and λ_r = 1.8033 μm chosen from the first and second peak of Fig. 4. Figure 9 and 10 show simulation snapshots of propagation of λ_s and λ_r, respectively, through the sensor structure for RI = 3.46 and 3.466.

Figure 9 clearly shows reduction in output transmission of λ_s = 1.7637 μm when the refractive index is varied from 3.46 to 3.466 in steps of 0.001.

Figure 10 clearly shows no change in output transmission of λ_r = 1.8033 μm when the refractive index is varied from 3.46 to 3.466.

Figures 11 and 12 show the changes in transmission with the variation of refractive index. We can clearly see from these two figures that the proposed sensor shows a vivid change in transmission with RI variation when the light of wavelength 1.7637 μm is

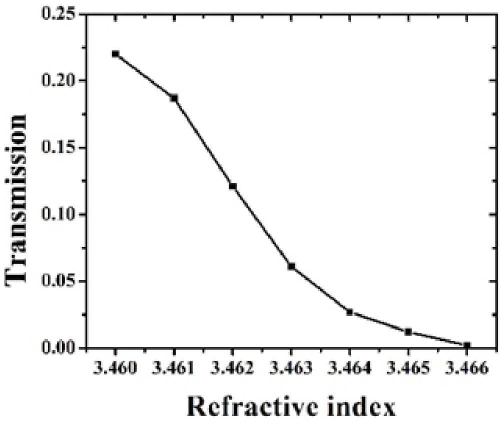

Fig. 11. Transmission *vs*. refractive-index for wavelength λ_s = 1.7637 μm.

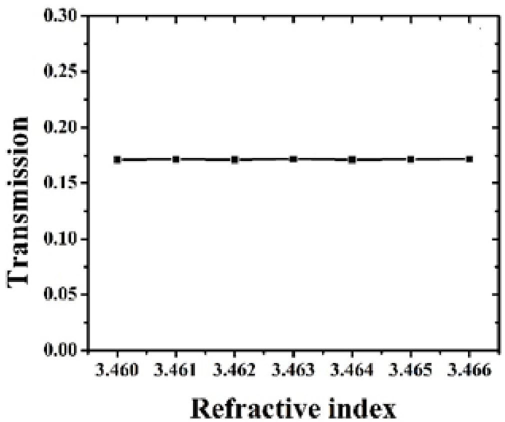

Fig. 12. Transmission *vs*. refractive-index for wavelength λ_r = 1.8033 μm.

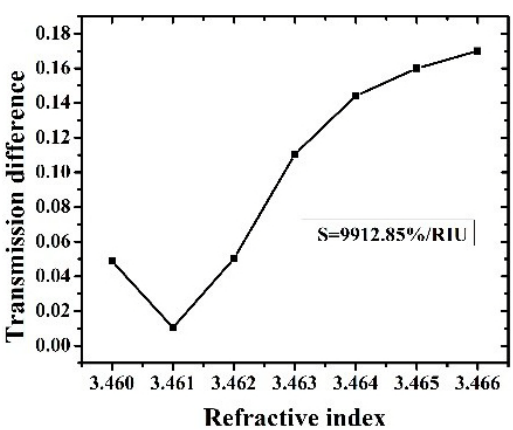

Fig. 13. Transmission difference *vs*. refractive-index.

T a b l e. Comparison of the proposed sensor with the other structures.

Reference	Authors	Quality factor
[41]	A. Parapurath, F. Alpeggiani, L. Kuipers, E. Verhagen	486
[42]	H. Alipour-Banaei, M. Jahnara, F. Mehedi Zadeh	707
[43]	M . Wu, Y. Yang, H. Fei, H. Lin, X. Zhao, L. Kang, L. Xiao	679.3
[44]	Rupali, S.K. Sahu, G. Palai, B.A. Kumar, B.K. Mishra	650
This work	N. Ghosh, P. Sharma, S. Medhekar	708.17

injected in the structure, while we observe no such change when the light of wavelength 1.8033 μm is used as input signal.

Figure 13 shows the change in the transmission difference between λ_r and λ_s with the variation of RI. The designed sensor exhibits a sensitivity of 9912.85%/RIU and a quality factor of 708.17.

Therefore, the considered structure can act as a dual resonance self-referenced refractive index sensor.

The Table presents a comparison of the proposed sensor with the other structures.

The advantage of the proposed sensor lies in the fact that it does not require another device to measure the effect of external factors (humidity *etc*.). The additional refractive index change due to these external factors can be measured from the transmission variation of the reference wavelength. The intensity variation in the case of reference wavelength will start increasing if the external factors come into play and by measuring those changes we can accurately measure the effect of these factors on the reading of the sensing wavelength and subtract it from the required data. So we can see that this type of sensor can be deployed in harsh environment without the need of any extra supporting equipment.

5. Conclusion

In the present work, we have designed and simulated intensity based dual resonance self-referenced refractive-index sensor in a 2D photonic crystal-based waveguide-cavity system. This method of sensing nullifies the effect of external factors increasing the accuracy of the results. The proposed sensor shows a sensitivity of 9912.85%/RIU and quality factor of 708.17. The sensitivity of the sensor is calculated by measuring the variation of the relative intensity difference with varying refractive-index. Being a very compact, the proposed sensor can easily be integrated in any system. However, the proposed sensor cannot sense biological and chemical analytes. The proposed sensor structure exhibits Fano-like spectral response and should have potential applications in different functionalities similar to applications of Fano resonance which should be a matter of further investigations.

Acknowledgements

Nilaksha Ghosh acknowledges the university fellowship provided by the Central University of Jharkhand, Ranchi, India.

References

[1] Wu Y., Zhou Y., Pan J, Huang T., Jin S.,*Design of highly sensitive refractive index sensor based on silicon photonic Mach–Zehnder interferometer*, Optics Communications **534**, 2023, 129288. https://doi.org/10.1016/j.optcom.2023.129288

[2] Rocco D., Tognazzi A., Gandolfi M., Carletti L., De Angelis C., Locatelli A., Cino A.C., *Refractive index sensing by a silicon metasurface*, 2022 IEEE 21st Mediterranean Electrotechnical Conference (MELECON), Palermo, Italy, 2022: 266-270. https://doi.org/10.1109/melecon53508.2022.9842969

[3] Hamdani M.A., Qazi G., *Modelling and theoretical analysis of a novel common mirror based silicon photonic Michelson modulator*, Optical and Quantum Electronics **55**, 2023: 41. https://doi.org/10.1007/s11082-022-04312-4

[4] Hamdani M.A., Qazi G., *Evaluating variability and improving tolerance in a novel and compact silicon photonic Michelson interferometer*, Silicon **14**, 2022: 9945-9958. https://doi.org/10.1007/s12633-022-01677-9

[5] Ziebell M., Marris-Morini D., Rasigade G., Fédéli J.-M., Crozat P., Cassan E., Bouville D., Vivien L., *40 Gbit/s low-loss silicon optical modulator based on a pipin diode*, Optics Express **20**(10), 2012: 10591-10596. https://doi.org/10.1364/oe.20.010591

[6] Thomson D.J., Gardes F.Y., Reed G.T, Milesi F., Fedeli J.-M.,*High speed silicon optical modulator with self aligned fabrication process*, Optics Express **18**(18), 2010: 19064-19069. https://doi.org/10.1364/oe.18.019064

[7] Dawood N.Y.M., Younis B.M., Areed N.F.F., Hameed M.F.O, Obayya S.S.A., *Mid-infrared optical modulator based on silicon D-shaped photonic crystal fiber with VO_2 material*, Applied Optics **60**(30), 2021: 9488-9496. https://doi.org/10.1364/ao.440371

[8] Singh J.J., Dhawan D., Gupta N., *2D photonic crystal hexagonal ring resonator-based all-optical logic gates*, Optics & Laser Technology **165**, 2023: 109624. https://doi.org/10.1016/j.optlastec.2023.109624

[9] Chanu S. A., Sonkar R. K., *High coupling efficiency photonic crystal waveguide for compact channel drop filter design on silicon-on-insulator platfor*, Optical Engineering **62**(8), 2023: 087101. https://doi.org/10.1117/1.oe.62.8.087101

[10] Chhipa M.K., Madhav B.T.P., Robinson S, Janyani V., Suthar B.,*Realization of all-optical logic gates using a single design of 2D photonic band gap structure by square ring resonator*, Optical Engineering **60**(7), 2021: 075104. https://doi.org/10.1117/1.oe.60.7.075104

[11] Kumar A., Medhekar S., *All optical NOR and NAND gates using four circular cavities created in 2D nonlinear photonic crystal*, Optics & Laser Technology **123**, 2020: 105910. https://doi.org/10.1016/j.optlastec.2019.105910

[12] Mirzaiee S., Noori M., Baghban H., Veladi H., *All-optical memory based on slow light and Kerr effect in photonic crystal platform with independent write/read/hold control*, Physica Scripta **97**(6), 2022: 065502. https://doi.org/10.1088/1402-4896/ac698e

[13] Zargarzadeh M., Yavari M.H., Heydari M., Rezaei M.H., *Refractive index sensor based on photonic crystal nanocavities*, 2021 29th Iranian Conference on Electrical Engineering (ICEE), Tehran, Islamic Republic of Iran, 2021: 39-42. https://doi.org/10.1109/icee52715.2021.9544255

[14] Maleki M.J., Soroosh M., *A novel proposal for performance improvement in two-dimensional photonic crystal-based 2-to-4 decoders*, Laser Physics **30**, 2020: 076203. https://doi.org/10.1088/1555-6611/ab9089

[15] Radhouene M., Najjar M., Chhipa M.K., Robinson S., Suthar B., *Design and analysis a thermo -optic switch based on photonic crystal ring resonator*, Optik **172**, 2018: 924-929. https://doi.org/10.1016/j.ijleo.2018.07.118

[16] Venkatachalam K., Kumar D.S., Robinson S., *Investigation on 2D photonic crystal-based eight -channel wavelength-division demultiplexer*, Photonic Network Communications **34**, 2017: 100-110. https://doi.org/10.1007/s11107-016-0675-7

[17] Biswas U., Rakshit J.K., Das. J., Bharti. G.K., Suthar B., Amphawan A., Najjar M., *Design of an ultra-compact and highly-sensitive temperature sensor using photonic crystal based single micro-ring resonator and cascaded micro-ring resonator*, Silicon **13**, 2021: 885-892. https://doi.org/10.1007/s12633-020-00489-z

[18] Sharma P., Medhekar S., *Ring resonator-based highly sensitive chemical/biochemical sensor created on holes in silicon slab 2D photonic crystal*, Journal of Optics **52**, 2023: 2315-2322. https://doi.org/10.1007/s12596-023-01149-2

[19] Miyan H., Agrahari R., Gowre S.K., Jain P.K., Mahto M., *Photonic crystal based ultrafast and highly sensitive refractive index sensor*, IEEE Sensors Journal **23**(14), 2023: 15563-15569. https://doi.org/10.1109/jsen.2023.3283506

[20] Nohoji A.H.A., Danaie M., *Highly sensitive refractive index sensor based on photonic crystal ring resonators nested in a Mach–Zehnder interferometer*, Optical and Quantum Electronics **54**, 2022: 574. https://doi.org/10.1007/s11082-022-04006-x

[21] Najafgholinezhad S., Olyaee S., *A photonic crystal biosensor with temperature dependency investigation of micro-cavity resonator*, Optik **125**(21), 2014: 6562-6565. https://doi.org/10.1016/j.ijleo.2014.08.043

[22] Zegadi R., Zegadi A., Zebiri C., Mosbah S., Mekki S., Bouknia M.L., Benjedi H., *Enhanced 2D photonic crystal sensor for high sensitivity sulfuric acid (H_2SO_4) and hydrogen peroxide (H_2O_2) detection*, Silicon **14**, 2022: 11001-11006. https://doi.org/10.1007/s12633-022-01836-y

[23] Peng F., Wang Z., Yuan G., Guan L., Peng Z., *High-sensitivity refractive index sensing based on Fano resonances in a photonic crystal cavity-coupled microring resonator*, IEEE Photonics Journal **10**(2), 2018: 6600808. https://doi.org/10.1109/jphot.2018.2815622

[24] Olyaee S., Najafgholinezhad S., Alipour Banaei H., *Four-channel label-free photonic crystal biosensor using nanocavity resonators*, Photonic Sensors **3**, 2013: 231-236. https://doi.org/10.1007/s13320-013-0110-y

[25] Zhao M., Wang J., Zhang Y., Ge M., Zhang P., Shen J., Li C., *Self-referenced refractive index sensor based on double-dips method with bimetal-dielectric and double-groove grating*, Optics Express **30**(5), 2022: 8376-8390. https://doi.org/10.1364/oe.454344

[26] Chowdhury U., Mukherjee R., Maity A.R., Kumar S., Maji P.S., *Self-referenced refractive index sensor utilizing Tamm plasmon in a photonic quasicrystal*, Optical and Quantum Electronics **55**, 2023: 869. https://doi.org/10.1007/s11082-023-05160-6

[27] Barrios C.A., Mirea T., Represa M.H., *A self-referenced refractive index sensor based on gold nanoislands*, Sensors **23**(1), 2023: 66. https://doi.org/10.3390/s23010066

[28] Srivastava S.K, Verma R, Gupta B.D., *Theoretical modeling of a self-referenced dual mode SPR sensor utilizing indium tin oxide film*, Optics Communications **369**, 2016: 131-137. https://doi.org/10.1016/j.optcom.2016.02.035

[29] Verma R., Srivastava S.K., *Self-referenced dual mode SPR sensing using sandwiched ITO layer: Long range vs. short range SPR referencing*, 13th International Conference on Fiber Optics and Photonics, December 4-8, 2016, Kanpur, India. https://doi.org/10.1364/PHOTONICS.2016.Th3A.79

[30] Kumar S., Shukla M.K., Maji P.S., Das R., *Self-referenced refractive index sensing with hybrid-Tamm-plasmon-polariton modes in sub-wavelength analyte layers*, Journal of Physics D: Applied Physics **50**(37), 2017, 375106. https://doi.org/10.1088/1361-6463/aa7fd7

[31] Zhang M., Ge C., Lu M., Zhang Z., Cunningham B.T., *A self-referencing biosensor based upon a dual-mode external cavity laser*, Applied Physics Letters **102**(21), 2013: 213701. https://doi.org/10.1063/1.4801427

[32] Abutoama M., Abdulhalim I., *Angular and intensity modes self-referenced refractive index sensor based on thin dielectric grating combined with thin metal film*, IEEE Journal of Selected Topics in Quantum Electronics **23**(2), 2017: 72-80. https://doi.org/10.1109/jstqe.2016.2520878

[33] Wang X., Zhu J., Xu Y., Qi Y., Zhang L., Yang H., Yi Z., *A plasmonic refractive index sensor with double self-reference characteristic*, Europhysics Letters **135**(2), 2021: 27001. https://doi.org/10.1209/0295-5075/135/27001

[34] VERMA S.K., SRIVASTAVA S.K., *High performance extra-ordinary transmission based self-referenced plasmonic metagrating sensor in NIR communication band*, Physica Scripta **98**(5), 2023: 055515. https://doi.org/10.1088/1402-4896/accb16

[35] WANG Y., SUN C., LI H., GONG Q., CHEN J., *Self-reference plasmonic sensors based on double Fano resonances*, Nanoscale **9**(31), 2017: 11085-11092. https://doi.org/10.1039/C7NR04259K

[36] SUN P., ZHOU C., JIA W., WANG J., XIANG C., XIE Y., ZHAO D., *Self-referenced refractive index sensor based on hybrid mode resonances in 2D metal-dielectric grating*, Journal of Physics D: Applied Physics **53**(14), 2020: 145101. http://doi.org/10.1088/1361-6463/ab6624

[37] PAN J., SRIVASTAVA S.K., *Simulation of a self-referenced meta grating sensor with high figure of merit in NIR communication window*, IEEE Sensors Journal **23**(8), 2023: 8344-8351. https://doi.org/10.1109/JSEN.2023.3250952

[38] SUN P., XIE Y., XIANG C., ZHAO D., WANG J., JEI W., ZHOU C., *Non-equidistant arrangement in all-dielectric quadrumers and mirror-symmetric one-dimensional photonic crystals hybridstructure for self-referenced sensing scheme*, Journal of Lightwave Technology **38**(23), 2020: 6671-6677. https://doi.org/10.1109/JLT.2020.3013672

[39] JOANNOPOULOS J.D., JOHNSON S.G., WINN J.N., MEADE R.D., *Photonic Crystals: Molding the Flow of Light*, Princeton University Press, 2008.

[40] LEUNG K.M., LIU Y.F., *Photon band structures: The plane-wave method*, Physical Review B **41**, 1990: 10188. https://doi.org/10.1103/physrevb.41.10188

[41] PARAPURATH A., ALPEGGIANI F., KUIPERS L., VERHAGEN E., *Direct observation of topological edge states in silicon photonic crystals: Spin,dispersion and chiral routing*, Science Advances **6**(10), 2020. https://doi.org/10.1126/sciadv.aaw4137

[42] ALIPOUR-BANAEI H., JAHNARA M., MEHEDIZADEH F., *Channel drop filter based on photonic crystal ring resonator*, Optica Applicata **48**(4), 2018: 601-608. https://doi.org/10.5277/oa180406

[43] WU M., YANG Y., FEI H., LIN H.,ZHAO X., KANG L., XIAO L., *On-chip ultra-compact hexagoanl boron nitride topological ring-resonator in visible region*, Journal of Lightwave Technology **40**(23), 2022: 7610-7618. https://doi.org/10.1109/JLT.2022.3203563

[44] RUPALI, SAHU S.K., PALAI G., KUMAR B.A., MISHRA B.K., *Modelling of photonic crystal based ring resonator sensor for cancer detection using infrared laser*, Journal of Optics, 2024. https://doi.org/10.1007/s12596-024-02107-2

Received June 5, 2024
in revised form September 29, 2024